Design, Implementation, and Demonstration of a Staggered PRT Algorithm for the WSR-88D

SEBASTIÁN M. TORRES AND YANNICK F. DUBEL

Cooperative Institute for Mesoscale Meteorological Studies, The University of Oklahoma, and National Severe Storms Laboratory, Norman, Oklahoma

DUSAN S. ZRNIĆ

National Severe Storms Laboratory, Norman, Oklahoma

(Manuscript received 23 December 2003, in final form 26 March 2004)

ABSTRACT

This paper describes the implementation of the staggered pulse repetition time (PRT) technique on NOAA's research and development WSR-88D in Norman, Oklahoma. The prototype algorithm incorporates a novel rule for the correct assignment of Doppler mean velocity that is needed to accommodate arbitrary stagger ratios. Description of the rule, consideration of errors, and choice of appropriate stagger ratios are presented. The staggered PRT algorithm is integrated with the standard processing on the WSR-88D, some details of which are included in the paper. A simple ground clutter canceller removes the pure complex time series mean (DC) component from autocovariance estimates; censoring of overlaid echoes and thresholding are equivalent to those used on the WSR-88D. Further, a cursory verification of statistical errors indicates good agreement with theoretical expectations. Although the staggered PRT algorithm operates in real time, it was advantageous to collect several events of staggered PRT time series data for further scrutiny. Results presented from one of the events demonstrate the potency of the staggered PRT to mitigate range and velocity ambiguities.

1. Introduction

It is well known that for Doppler radars transmitting uniformly spaced pulses there is a coupling between the maximum unambiguous range (r_a) and the maximum unambiguous velocity (v_a); r_a or v_a can only be increased at the expense of a proportional decrease in the other (Doviak and Zrnić 1993). This is a fundamental limitation for the observation of severe weather. Various schemes have been proposed to mitigate the effects of ambiguities, but few have been tested and even fewer are available on operational weather radars. Examples of these are random phase coding and dual pulse repetition frequency (PRF), which have been tested and are commercially available (Joe et al. 1997; Joe and May 2003).

Several mechanisms are currently provided to alleviate effects of range overlaid echoes and velocity aliasing in the Weather Surveillance Radar-1988 Doppler (WSR-88D). At the lowest elevations, the WSR-88D performs two scans at each elevation angle. Each of these pairs of cuts is usually referred to as a ''split cut.'' The first scan uses a long pulse repetition time (PRT) and produces power (reflectivity) estimates up to 460 km. Doppler velocity estimates from this scan are almost useless due to their low maximum unambiguous velocity (about 9 m s^{-1}). The second scan at the same elevation angle uses a short PRT with a maximum unambiguous range of 148 km and produces (possibly range folded) unambiguous velocities in the range ± 28 m s^{-1}. At intermediate elevation angles, where clutter rejection requirements are less stringent, the WSR-88D reduces the time by running just one scan in the ''batch mode'' whereby long-PRT and short-PRT blocks of pulses are interlaced. Analogously to the split cut processing, powers are obtained from pulses at the long PRT ($r_a > 230$ km) and velocities from the short-PRT batch ($v_a = 28$ m s^{-1}). In both split cuts and batch mode, signal processing algorithms in the radar data acquisition (RDA) subsystem of the WSR-88D use the long-PRT power data to position velocity estimates from the short-PRT scan to the range location of the strongest trip echo. However, this algorithm fails in regions where the overlaid trip powers in the short-PRT scan are within 5 dB of each other. Therefore, the WSR-88D cannot recover velocities from the weaker trips or resolve strong overlays. Doppler velocity displays characterize these failures by encoding locations of such overlaid powers with a purple color, normally referred to as the ''purple haze.''

Corresponding author address: Sebastián M. Torres, National Severe Storms Laboratory, 1313 Halley Circle, Norman, OK 73069.
E-mail: sebastian.torres@noaa.gov

Over the last decade, the staggered PRT technique has emerged as a viable candidate to address the mitigation of range and velocity ambiguities in the WSR-88D thus reducing the amount of purple haze obscuration currently encountered during the observation of severe phenomena (Zrnić and Cook 2002). Its greatest potential is at intermediate elevations where ground clutter contamination is not a major concern. Using staggered PRTs in the context of weather surveillance radars was first proposed by Sirmans et al. (1976). With this technique, transmitter pulses are spaced at alternating PRTs T_1 and T_2. The staggered PRT ratio is defined as $\kappa = T_1/T_2$, which can be expressed as the ratio of two relatively prime integers m/n because the PRTs are derived from the same system clock. Lag-one autocorrelation estimates are made independently for each PRT, and these estimates are suitably combined so that the effective maximum unambiguous velocity can be extended.

This paper describes the design, real-time implementation, and demonstration of the staggered PRT sampling and processing on the National Severe Storms Laboratory's (NSSL) WSR-88D research radar. Unlike many of the algorithms described in the literature (Sirmans et al. 1976; Doviak et al. 1976, 1978; Zrnić and Mahapatra 1985; Doviak and Zrnić 1993; Loew and Walther 1995), our velocity dealiasing algorithm extends v_a to its theoretical maximum and is valid for any PRT ratio κ. The algorithm is derived from a careful study of the velocity difference transfer function that avoids a number of incorrect generalizations found in previous works. The staggered PRT technique has been thoroughly analyzed using theoretical and simulation studies, and a few tests have been made on research radars (e.g., a real-time implementation of a limited velocity dealiasing algorithm with no clutter filtering was briefly reported by Gray et al. 1989). However, no operational weather radar has the staggered PRT mode[1] (Holleman and Beekhuis 2003). Our recent real-time implementation of this algorithm made it possible to evaluate its performance under practical conditions. A description of this implementation is provided, and preliminary results on weather data are compared with those obtained via legacy processing techniques.

2. Maximum unambiguous velocity extension

Herein we briefly review the staggered PRT scheme and provide a rigorous explanation of the velocity dealiasing procedure. In addition, we discuss constraints on the errors of estimates and related modifications to the velocity dealiasing algorithm.

[1] A block-staggered mode in which two sequences of relatively close PRTs alternate is operational on the weather channel of ASR-9 radars, and effective clutter filters have been designed for these transmission sequences (Chornoboy 1993).

a. The staggered PRT technique

Staggered PRT sweeps are characterized by a transmission sequence that alternates two PRTs, T_1 and T_2, for a total of M pulses (without loss of generality, we assume that $T_1 < T_2$). Maximum unambiguous velocities corresponding to the short and long PRTs are given by $v_{a1} = \lambda/4T_1$ and $v_{a2} = \lambda/4T_2$, respectively, where λ is the radar wavelength. The maximum unambiguous range for the short PRT is $r_{a1} = cT_1/2$ and for the long PRT is $r_{a2} = cT_2/2$, where c is the speed of light. Taken by themselves (in a uniform PRT), the products of unambiguous range and velocity at either PRT satisfy the well-known equation given by

$$r_{a1}v_{a1} = r_{a2}v_{a2} = c\lambda/8. \tag{1}$$

Extension of unambiguous velocity beyond this constraint is the subject of the next section.

b. The Doppler velocity dealiasing algorithm

Doppler velocities v_1 and v_2 can be computed from the argument of lag-one autocorrelation estimates R_1 and R_2 (corresponding to the short and long PRTs, respectively) as

$$v_1 = -\frac{\lambda}{4\pi T_i}\,\mathrm{Arg}(R_i); \qquad i = 1, 2, \tag{2}$$

where Arg(·) denotes the principal argument restricted to the range $(-\pi, \pi]$. Because v_1 and v_2 alias on different Nyquist intervals (given by v_{a1} and v_{a2}, respectively), their difference can be used to resolve the true Doppler velocity in a larger interval. For a set of PRTs satisfying the relation $T_1/T_2 = m/n$, Nathanson (1969) states (without proof) that the $v_1 - v_2$ velocity difference remains unambiguous in the interval $\pm nv_{a1}$ (or $\pm mv_{a2}$). However, he fails to mention that this is true only for relatively prime integers m and n; the same omission occurs in the works of Sirmans et al. (1976), Doviak et al. (1976), Doviak et al. (1978), and Doviak and Zrnić (1993).

The Chinese remainder theorem (CRT) is used next to prove that the maximum unambiguous interval in which the true Doppler velocity v can be resolved is indeed as given by Nathanson if m and n are relatively prime integers. The lag-one autocorrelation function of weather signals is of the form [cf. (6.4) of Doviak and Zrnić 1993]

$$R_i = S\rho(T_i)\exp(-j4\pi vT_i/\lambda); \; i = 1, 2, \tag{3}$$

where S is the signal power and ρ is the magnitude of the normalized signal correlation. Then,

$$\mathrm{Arg}(R_i) \equiv -\frac{4\pi vT_i}{\lambda}(\mathrm{mod}\ 2\pi); \qquad i = 1, 2, \tag{4}$$

where $\equiv$ denotes modulo (mod) congruence. Multiplying this equation by $n/2\pi$ and $m/2\pi$ for $i = 1$ and 2, respectively, produces

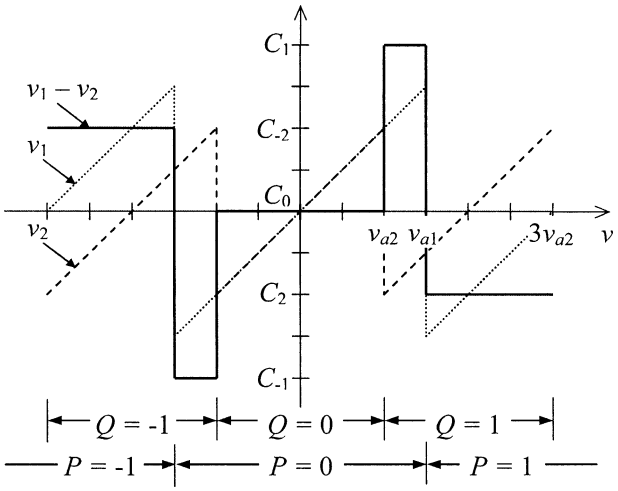

FIG. 1. Aliased Doppler velocities v_1 and v_2 and the velocity difference transfer function $(v_1 - v_2)$ as a function of the true Doppler velocity v for $\kappa = 2/3$. The Nyquist interval numbers for v_1 and v_2 are indicated by P and Q, respectively.

$$-\frac{2vnT_1}{\lambda} \equiv \frac{\text{Arg}(R_1)}{2\pi} n(\text{mod } n),$$
$$-\frac{2vmT_2}{\lambda} \equiv \frac{\text{Arg}(R_2)}{2\pi} m(\text{mod } m). \quad (5)$$

Because the two expressions on the left side of (5) are equal ($T_1/T_2 = m/n$), and m and n are relatively prime integers, the CRT (Ding et al. 1996) applies to the integer parts of the terms in that equation (the fractional parts of all the terms must be the same so the congruencies still hold). Therefore, a unique value of $-2vnT_1/\lambda$ (or $-2vmT_2/\lambda$) can be determined in the interval $[0, mn)$, which is equivalent to saying that v can be unambiguously resolved in the range $\pm v_a$ where

$$v_a = mv_{a1} = nv_{a2}. \quad (6)$$

The goal, then, is to use the staggered PRT technique to achieve the maximum theoretical extension of v_a given in (6).

Two approaches to dealias velocity estimates in the context of staggered PRT have been discussed in the literature. One technique uses the argument of the ratio of short- and long-PRT lag-one autocorrelations (Zrnić and Mahapatra 1985; Doviak and Zrnić 1993; Sachidananda and Zrnić 2000) as

$$v = \frac{\lambda}{4\pi(T_2 - T_1)} \text{Arg}\left(\frac{R_1}{R_2}\right). \quad (7)$$

Velocity estimates become ambiguous if the true argument of R_1/R_2 is outside the interval $\pm\pi$; that is, the maximum unambiguous velocity obtained with this method is $\lambda[4(T_2 - T_1)]^{-1} = (1 - \kappa)^{-1}v_{a2}$. In general, (7) cannot be used to extend the maximum unambiguous velocity to the theoretical maximum in (6) because the individual arguments of R_1 and R_2 are lost when combined in the ratio. Maximum extension of v_a is achieved only if $(1 - \kappa)^{-1} = n$ [cf. (6)]; i.e., for stagger ratios of the form $\kappa = m/(m + 1)$.

A rule-based technique that achieves extension of the maximum unambiguous velocity to the theoretical limit in (6) was introduced by Sirmans et al. (1976). Founded on the properties of the velocity difference transfer function $(v_1 - v_2)(v)$, the algorithm uses the values of $v_1 - v_2$ to define ''dealiasing rules.'' Nonetheless, the rules in this and other works (Loew and Walther 1995; Sachidananda and Zrnić 2002) turn out to be valid only for specific PRT ratios. To address these deficiencies, we introduce relevant properties of the velocity difference transfer function, and from these, we derive a set of dealiasing rules applicable to any PRT ratio. This has more than academic interest because the currently available PRTs on the WSR-88D network form none of the specific ratios for which the rules had been previously derived.

1) THE VELOCITY DIFFERENCE TRANSFER FUNCTION

Using the fact that $v_1(v)$ aliases on $\pm v_{a1}$ and $v_2(v)$ on $\pm v_{a2}$, the velocity difference transfer function can be obtained as

$$(v_1 - v_2)(v) = \left[2v_{a1}\,\text{frac}\left(\frac{v + v_{a1}}{2v_{a1}}\right) - v_{a1}\right] - \left[2v_{a2}\,\text{frac}\left(\frac{v + v_{a2}}{2v_{a2}}\right) - v_{a2}\right], \quad (8)$$

where both $v_1(v)$ and $v_2(v)$ are sawtooth functions and frac(x) is the fractional part of x. It is not difficult to prove that this function is odd and $2v_a$ periodic, where v_a is given in (6). In addition, it is piecewise constant; its discontinuity points are brought about by the frac functions and are of the form $(2k - 1)v_{a1}$ and $(2k - 1)v_{a2}$, where k is an integer. The function takes $2L + 1$ constant values $\{C_l, -L \le l \le L\}$ in $(-v_a, v_a)$, where L is $(m + n - 2)/2$ for odd m and n and $(m + n - 1)/2$ otherwise (Torres et al. 2004, unpublished manuscript). Thus, (8) can be rewritten as

$$(v_1 - v_2)(v) = \sum_{l=-L}^{L} C_l I_l(v), \quad (9)$$

where

$$I_l(v) = \begin{cases} 1 & v_l^{(d)} \le v < v_{l+1}^{(d)}, \\ 0 & \text{otherwise}, \end{cases} \quad (10)$$

and $v_l^{(d)}$ are the discontinuity points of $(v_1 - v_2)(v)$ in $[-v_a, v_a)$, such that $-v_a = v_{-L}^{(d)} < v_{-L+1}^{(d)} < \cdots < v_{L+1}^{(d)} = v_a$. Finally, it can be proved that the constant values C_l are all different and, if sorted, they are evenly spaced at $\Delta_C = 2v_a/mn$ (Torres et al. 2004, unpublished manuscript). An example of the velocity difference transfer function for $\kappa = 2/3$ is given in Fig. 1.

2) The dealiasing rules

According to the properties of the velocity difference transfer function given in (9), there is a bijection between $\{C_l, -L \le l \le L\}$ and $\{I_l, -L \le l \le L\}$. Therefore, the value of $v_1 - v_2$ (matching a particular C_l) can be used to determine the correct interval (i.e., the I_l corresponding to C_l) of the true Doppler velocity. The dealiasing rules associate values of $v_1 - v_2$ with adjustment factors that bring v_1 (or v_2) to its correct Nyquist interval. In other words, a set of dealiasing rules lists the possible values of C_l and the correct Nyquist interval number $P_l(Q_l)$ for $v_1(v_2)$ so that the dealiased velocity is computed as $v = v_1 + 2P_l v_{a1}$ ($v = v_2 + 2Q_l v_{a2}$). Although the discontinuity points of $(v_1 - v_2)(v)$ are always of the form $(2k - 1)v_{a1}$ or $(2k - 1)v_{a2}$, the way in which they are sorted to form the sequence $\{v_l^{(d)}, -L \le l \le L + 1\}$ depends on the value of κ. Hence, there is a unique set of dealiasing rules for each PRT ratio.

A general set of dealiasing rules can be derived by examining the function $(v_1 - v_2)(v)$ in the interval $\pm v_a$. Because this function is odd, we can concentrate on the positive velocities first and then extend the results using the symmetry of the function. In the neighborhood of $v = 0$ neither v_1 nor v_2 are aliased; hence, $C_0 = 0$, $P_0 = 0$, and $Q_0 = 0$. This holds until the true velocity reaches the first discontinuity point ($v_l^{(d)}$). As we move away from zero velocity, $(v_1 - v_2)(v)$ jumps to a different constant value at each discontinuity point. If the discontinuity point is of the form $(2k - 1)v_{a1}$, $(v_1 - v_2)(v)$ changes by $-2v_{a1}$ since we have moved to a different Nyquist interval of v_1 (P_l is incremented). On the other hand, if the discontinuity point is of the form $(2k - 1)v_{a2}$, the function changes by $2v_{a2}$ and we are in a new Nyquist interval of v_2 (Q_l is incremented). Therefore, the $2L + 1$ dealiasing rules that correspond to the $2L + 1$ constant values of $(v_1 - v_2)(v)$ are recursively determined using the following algorithm:

1) $C_0 = 0$, $P_0 = 0$, $Q_0 = 0$.
2) For $l = 1, 2, \ldots, L$.

If $v_l^{(d)}$ is of the form $(2k - 1)v_{a1}$: $C_l = C_{l-1} - 2v_{a1}$, $P_l = P_{l-1} + 1$, $Q_l = Q_{l-1}$.

If $v_l^{(d)}$ is of the form $(2k - 1)v_{a2}$: $C_l = C_{l-1} + 2v_{a2}$, $P_l = P_{l-1}$, $Q_l = Q_{l-1} + 1$.

3) For $l = -1, -2, \ldots, -L$,

$$C_l = -C_{-l},\ P_l = -P_{-l},\ Q_l = -Q_{-l}.$$

For example, for $\kappa = 2/3$ the velocity difference transfer function is depicted in Fig. 1. The discontinuity points of $(v_1 - v_2)(v)$ in $[-v_a, v_a]$ are $-3v_{a2}$, $-v_{a1}$, $-v_{a2}$, v_{a2}, v_{a1} and $3v_{a2}(L = 2)$. The dealiasing rules obtained with this algorithm are given in Table 1.

TABLE 1. Dealiasing rules for $\kappa = 2/3$.

l	C_l	P_l	Q_l
−2	$-2v_{a2} + 2v_{a1}$	−1	−1
−1	$-2v_{a2}$	0	−1
0	0	0	0
1	$2v_{a2}$	0	1
2	$2v_{a2} - 2v_{a1}$	1	1

3) Consideration of errors

In practice, v_1 and v_2 will exhibit unavoidable estimation errors. In that case, the value of $v_1 - v_2$ may not match any of the theoretical constant levels of the velocity difference transfer function, and we must choose the C_l that minimizes $|v_1 - v_2 - C_l|$. Statistical errors in v_1 and v_2 cause $v_{1d} = v_1 + 2P_l v_{a1}$ and $v_{2d} = v_2 + 2Q_l v_{a2}$ to be different and, in general, the dealiased Doppler velocity should be computed as $v = \alpha v_{1d} + (1 - \alpha)v_{2d}$ (e.g., $\alpha = 0.5$ results in the average of the dealiased velocities). If the errors of estimates are known, an optimum value of α in the minimum-mean-square-error sense can be determined. However, the variance of v_1 estimates is smaller than for v_2 because $T_1 < T_2$ [cf. (6.21) of Doviak and Zrnić 1993], and in practice, the dealiased Doppler velocity can be approximated as $v \approx v_{1d}(\alpha = 1)$.

If the errors in v_1 and v_2 are too large, the C_l obtained by minimizing $|v_1 - v_2 - C_l|$ may not be the one obtained in an error-free situation. Choosing the wrong C_l leads to "catastrophic errors" because the Doppler velocity is dealiased into the wrong Nyquist interval. To avoid catastrophic errors, the maximum error in $v_1 - v_2$ should be less than one-half of the minimum spacing between any two constant levels of the velocity difference transfer function. That is, from the variance of $v_1 - v_2$ estimates, $\mathrm{var}(v_1 - v_2) = \mathrm{var}(v_1) + \mathrm{var}(v_2) - 2\mathrm{cov}(v_1, v_2)$ (Papoulis 1984), we have that $\mathrm{var}(v_1 - v_2) < 2\mathrm{var}(v_2)$ [because under normal conditions $\mathrm{cov}(v_1, v_2) > 0$ (Zrnić 1977) and $\mathrm{var}(v_1) < \mathrm{var}(v_2)$] and the condition becomes $\sqrt{2}\mathrm{SD}(v_2) < \Delta_C/2 = v_a/mn$. Therefore, the maximum allowable error of velocity estimates to avoid catastrophic errors is given by

$$e_{\max} = v_a/\sqrt{2}mn. \tag{11}$$

For example, to allow catastrophic errors only 0.5% of the time, the standard deviation of velocity estimates should be at least 2 times smaller than $e_{\max}$. These few remaining errors can be easily removed by techniques based on field continuity such as the velocity dealiasing algorithm implemented in the WSR-88D radar product generation (RPG) subsystem.

If m and n are large, the maximum allowable error of velocity estimates becomes unrealistically small. To avoid this, fewer dealiasing rules can be used to artificially increase Δ_C at the cost of reducing the range of recoverable Doppler velocities. That is, rules are dropped in pairs beginning at the ends of the interval

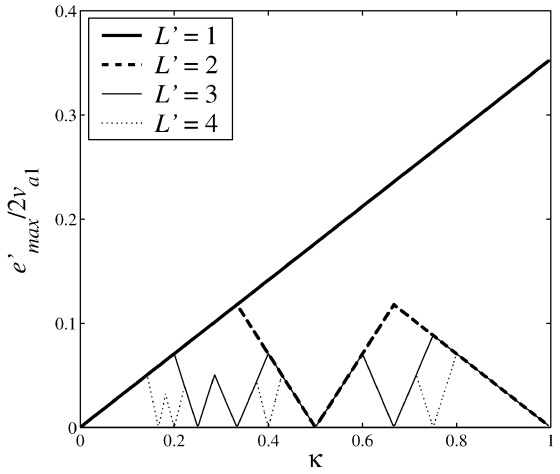

FIG. 2. Normalized maximum allowable error of velocity estimates ($e'_{max}/2v_{a1}$) vs the staggered PRT ratio (κ) for different values of L'. The maximum allowable error is computed as $e'_{max} = \Delta_C(L')/\sqrt{8}$, where $\Delta_C(L')$ is the minimum spacing between the constant levels of the velocity difference transfer function $(v_1 - v_2)(v)$ in the interval $\pm v^{(d)}_{L'+1}$ (i.e., using $L' \leq L$ dealiasing rules).

$\pm v_a$ toward zero velocity until Δ_C becomes acceptable. Because dropping a pair of rules does not always guarantee an increase in Δ_C, larger errors of estimates may force a significant reduction in the effective maximum unambiguous velocity. The algorithm described before can be modified accordingly by reducing the range of l to $L' \leq L$ in step 2 and to $-L'$ in step 3. With this change, $\Delta_C = \Delta_C(L')$, and the effective maximum unambiguous velocity becomes $v^{(d)}_{L'+1}$. Further, velocities that are larger than $v^{(d)}_{L'+1}$ are assigned to the wrong interval creating catastrophic errors. In general, these errors are not isolated as in the previous case and cannot be easily removed by techniques based on field continuity.

Figure 2 shows the normalized maximum allowable error of velocity estimates versus the staggered PRT ratio for different values of L'. In general, it can be verified that for a fixed κ the effective maximum allowable error of velocity estimates, $e'_{max} = \Delta_C(L')/\sqrt{8}$, increases as L' decreases, that is, as more dealiasing rules are dropped. If only three rules are used ($L' = 1$), $\Delta_C(1) = 2v_{a2}$ because for any value of κ, $C_{-1} = -2v_{a2}$, $C_0 = 0$, and $C_1 = 2v_{a2}$. Therefore, $e'_{max} = v_{a2}/\sqrt{2}$, and its normalized counterpart is linear with $\kappa(e'_{max}/2v_{a1} = \kappa/\sqrt{8})$. If more rules are used, the general expression of e'_{max} for a given κ is $e'_{max} = (pv_{a1} + qv_{a2})/\sqrt{2}$ (p and q integers) because C_l are of the form $-2P_l v_{a1} + 2Q_l v_{a2}$. Then, $e'_{max}/2v_{a1} = (p + q\kappa)/\sqrt{8}$ and the curves of $e'_{max}/2v_{a1}$ are piecewise linear with the slopes determined by the value of q.

The plot in Fig. 2 can be used to determine the optimum value of L' for a given situation. For example, consider the case where the PRTs are such that $\kappa = 2/3$ and $v_{a1} = 10$ m s^{-1}, the standard deviation of velocity estimates using the long PRT is $SD(v_2) = 1$ m s^{-1}, and the probability of catastrophic errors should be under 0.5%. Then, the normalized maximum allowable error of velocity estimates is $e'_{max}/2v_{a1} = 2SD(v_2)/2v_{a1} = 0.1$, and from the plot in Fig. 2, two values of L', $L' = 1$ and $L' = 2$, are found to guarantee the desired performance for $\kappa = 2/3$. Whereas $L' = 1$ (three dealiasing rules) is acceptable in terms of occurrence of catastrophic errors, the effective maximum unambiguous velocity is only $v^{(d)}_2 = v_{a1} = 10$ m s^{-1}. The best choice in this situation is $L' = L = 2$ (five dealiasing rules), which results in a larger maximum unambiguous velocity given by $v^{(d)}_3 = 3v_{a2} = 20$ m s^{-1}. In general, the optimum velocity dealiasing algorithm should use the largest number of dealiasing rules (resulting in the largest effective v_a) that also ensures the required level of errors.

Figure 2 is also useful to quantify the improvement on the maximum allowable error of velocity estimates realized by systematically dropping pairs of rules (reducing L') for a given PRT ratio. Consider, for example, PRT ratios of the form 2/3, 3/4, and 4/5, which are among the most common choices for κ. If $\kappa = 2/3$, the maximum theoretical number of dealiasing rules is five and $L = 2$. Figure 2 confirms that dropping a pair of rules (going from $L = 2$ to $L' = 1$) results in immediate benefits since there is an increase in the normalized maximum allowable error of velocity estimates. Conversely, for both $\kappa = 3/4(L = 3)$ and $\kappa = 4/5(L = 4)$, benefits from cutting back pairs of rules are not realized until $L' = 1$; therefore, dropping just one pair of rules does not improve the algorithm performance in either case. These examples demonstrate that decreasing the number of dealiasing rules does not always guarantee an increase in the maximum allowable error of velocity estimates.

3. Implementation on the WSR-88D

a. Real-time environment

The NSSL has recently demonstrated a prototype of a replacement RDA front-end for the WSR-88D system based largely on commercial off-the-shelf (COTS) hardware (Zahrai et al. 2002). This prototype is integrated into the KOUN radar in Norman, Oklahoma, and is hereafter referred to as the research RDA (RRDA). Generally, the RRDA consists of three main components. A single-board host computer performs real-time monitoring and control functions. A synchronizer generates timing signals and triggers for the transmitter, receiver, and all built-in test and calibration equipment. Finally, a highly scalable multiprocessor engine with its own high-speed interconnect fabric implements all digital signal processing functions. The multiprocessor system consists of a number of boards from Mercury Computer Systems running MC/OS (Mercury's real-time operating system). Processors on these boards are PowerPC 7400 running at 400 MHz, each with 256 MB of memory, and linked together via Mercury's RACEWay crossbar

interconnect. Some of the most important features of the RRDA are its flexibility and expandability along with its capability to record up to 8 h of continuous time series data. In-phase (I) and quadrature-phase (Q) components and the corresponding metadata can be recorded with no interruptions onto a 135-GB disk array via a fiber channel interface.

Implementation of the staggered PRT algorithm required close cooperation between the sequencer module in the synchronizer, the host computer, and the signal processor. The functionality of the sequencer was expanded to enable the generation and acquisition of time series with staggered patterns. Further, the legacy set of eight PRTs was expanded so that new ones can be defined as multiples of the 9.6-MHz clock cycle. This allows generating staggered PRT sequences with any desired PRT ratio and maximum unambiguous range. Finally, the staggered PRT algorithm described above was tailored for a seamless integration into the legacy signal processing pipeline (Torres and Zahrai 2002). That is, even though the implementation incorporates new functionality (e.g., clutter filtering, velocity dealiasing, data censoring), it matches the legacy WSR-88D functionality when appropriate (e.g., interference suppression, strong point clutter censoring).

b. The staggered PRT algorithm

Herein we describe the staggered PRT algorithm that was implemented and tested on the research and development WSR-88D in Norman, Oklahoma. As the scheme is integrated into the standard (legacy) processing, certain details of interaction between the staggered PRT algorithm and the existing computations are also explained (e.g., preprocessing). In this implementation, we assume that there are no storms beyond r_{a2}. That is, echoes from the short PRT can overlay the ones from the long PRT, but not vice versa. This condition can always be satisfied at some elevation angle, but other considerations also influence the choice of r_{a2} (see section 4). A technique to resolve more complex overlay situations is given by Sachidananda and Zrnić (2003).

1) PREPROCESSING

Incoming I and Q data are corrected for automatic gain control (AGC) imperfections and phase detector imbalances. In addition, data showing interference are removed to avoid moment estimate biases. Power (P_1, P_2) and lag-one pulse-pair autocorrelation (R_1, R_2) arrays are computed for T_1 and T_2. While P_2 is computed up to r_{a2}, P_1, R_1, and R_2 can only be computed up to r_{a1}.

Next, a simple map-based clutter filter is applied to the two sets of autocovariance estimates. Following the approach by Anderson (1981), the clutter filtering algorithm removes (from the powers and real part of lag-one autocorrelations) the magnitude squared of the complex time series mean (or DC) component in those locations where the site-dependent clutter filter bypass map indicates the presence of ground clutter. Strong point clutter is also removed from powers and autocorrelation vectors. Whereas ground clutter filtering requirements in the WSR-88D mandate user-selectable suppression levels between 30 and 50 dB, suppression of this simple staggered PRT ground clutter filter is limited to about 10 dB. Hence, the greatest potential for this technique is at intermediate elevations where ground clutter is not a major concern. To extend the applicability of this algorithm to lower elevation angles and/or sites where ground clutter contamination is still a problem at higher elevations, Sachidananda and Zrnić (2002) proposed a novel, yet complex ground clutter filtering scheme that achieves the required suppression. Still, implementation of such a filtering scheme involves computationally intensive processing in the frequency domain. Although excellent results have been obtained on simulated signals with the staggered ratio 2/3, extension to other ratios may not be as favorable.

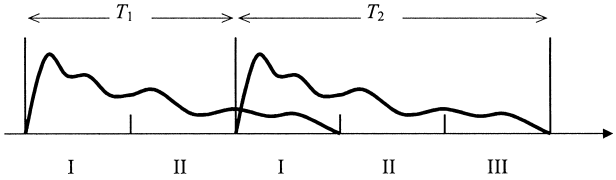

FIG. 3. Signal powers along range for illustration of the staggered PRT algorithm. Roman numerals indicate segment numbers used in the reflectivity computation and censoring.

2) DOPPLER VELOCITY DEALIASING

Doppler velocities v_1 and v_2 are estimated from lag-one autocorrelation arrays R_1 and R_2, and the velocity difference $v_1 - v_2$ is processed by the velocity dealiasing algorithm described in section 2. A table with the dealiasing rules is precomputed for the needed stagger ratio. This table consists of all the theoretical values of the velocity difference transfer function, where each of these values is associated with the correct Nyquist interval number for v_1. A dealiased velocity estimate is simply obtained as $v = v_1 + 2Pv_{a1}$, where P is the Nyquist interval number corresponding to the value in the table that best matches the measured $v_1 - v_2$.

3) REFLECTIVITY AND SPECTRUM WIDTH COMPUTATIONS

In addition to Doppler velocity, the WSR-88D produces estimates of reflectivity and spectrum width. To compute the reflectivity, data are extracted from the two power arrays P_1 and P_2 with different rules for each of the three segments depicted in Fig. 3. For segment I, data are extracted only from P_1 because P_2 may be contaminated at these range locations with overlaid

powers. An average of P_1 and P_2 is extracted for segment II, given that both power vectors are assumed to be ''clean'' there. Finally, segment III data are obtained from P_2. The spectrum width is computed as in the legacy WSR-88D [cf. (6.27) of Doviak and Zrnić 1993] but only using the powers and lag-one autocorrelations corresponding to the long PRT (T_2), which yield lower errors of estimates (Zrnić and Mahapatra 1985).

4) POSTPROCESSING

Before producing a final output, the WSR-88D RDA validates all spectral moment estimates. Censoring is applied to those range locations in which overlaid echoes have been detected, and thresholding to those in which the power is insufficient to be considered a significant return.

Censoring of velocity and spectrum-width data is only necessary in segment I. This is done by analyzing P_1 in segment I and P_2 in segment III (cf. Fig. 3). The idea is to determine whether second-trip signals mask first-trip signals in segment I of P_2. While such overlaid echoes appear in every other pulse and do not bias velocity estimates at those range locations, overlaid powers act as noise. Therefore, when second-trip powers in segment I of P_2 are above a preset fraction of their first-trip counterparts, the corresponding velocity and spectrum width estimates exhibit very large errors and must be censored.

As a final step, all moments are thresholded based on the signal-to-noise ratio (SNR), and data are scaled and formatted to be received, displayed, and processed by the RPG subsystem.

4. Performance of the staggered PRT algorithm

The performance of the staggered PRT algorithm described in the section 3 is directly tied to the selected set of PRTs. In a practical setting, the PRTs are constrained by both system and performance requirements. Hence, we first address the choice of PRTs and then examine the statistical performance of the algorithm as well as results on data.

a. Choice of PRTs

Figure 4 contains a concise plot of constraints of the WSR-88D. The square denoted by (I) corresponds to the system limitations on the PRT values. Currently, the minimum PRT that a WSR-88D transmitter can sustain is 760 μs. Further, signal processing memory allocation constraints limit the PRT to a maximum value of 3.14 ms, which is sufficient to observe storms within 460 km of the radar. The horizontal and vertical lines denoted by (II) correspond to range coverage constraints. That is, whereas the short PRT dictates the maximum unambiguous range to which Doppler velocity and spectrum width can be recovered, the long PRT determines

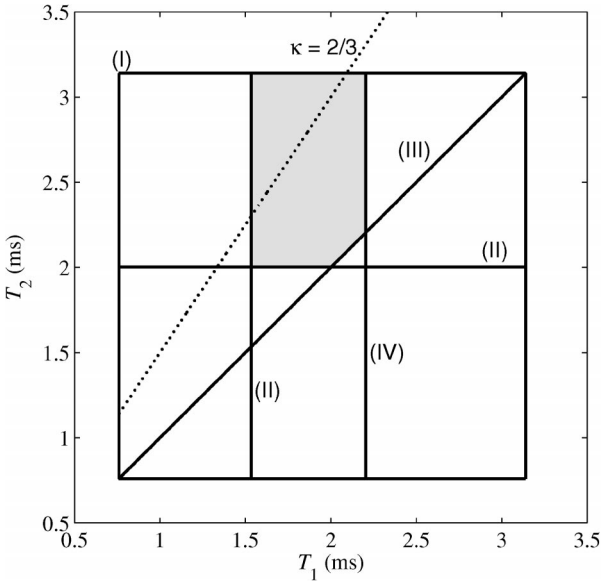

FIG. 4. Valid region of staggered PRTs for the WSR-88D. Solid lines indicate system (I), range coverage (II), design (III), and echo coherency constraints (IV). The dotted line represents the set of PRTs with a ratio $\kappa = 2/3$.

range coverage for the reflectivity. For intermediate elevation angles (between 2.4° and 6.2°) reflectivity coverage does not need to exceed $r_{\max}^{(S)} = 300$ km (assuming that most storms do not extend to a height above 18 km), thus limiting T_2 to values larger than $2r_{\max}^{(S)}/c \approx 2$ ms. On the other hand, requirements for recovery of Doppler velocity specify $r_{\max}^{(D)} = 230$ km, which limits T_1 to values larger than $2r_{\max}^{(D)}/c \approx 1.53$ ms. A design constraint is given by (III) because we assume that $T_1 < T_2$. Finally, echo coherency is achieved when the spectrum width (σ_v) is much smaller than the Nyquist interval (Doviak et al. 1978), which leads us to consider the inequality $T_1 < \lambda/4\pi\sigma_v$ denoted by (IV) (using a mean value of 4 m s^{-1} for σ_v). These constraints define the valid set of PRTs (shaded in gray in Fig. 4) that can be selected for the WSR-88D. For a given staggered PRT ratio ($\kappa = 2/3$ is plotted as a dotted line in Fig. 4), the shortest possible PRTs inside the valid region provide the best performance (largest v_a) and the ability to measure larger spectrum widths. Still, after selecting the PRT set from Fig. 4, Fig. 2 should be used to determine the corresponding maximum allowable error of velocity estimates, which is needed to adjust the required equivalent number of independent samples (M_I) and/or the number of dealiasing rules for the algorithm (L').

b. Statistical performance

The statistical performance of the velocity dealiasing algorithm is obtained using data collected with a stationary antenna. Figure 5 shows the results on a set of 200 radials of weather data recorded on 16 May 2003

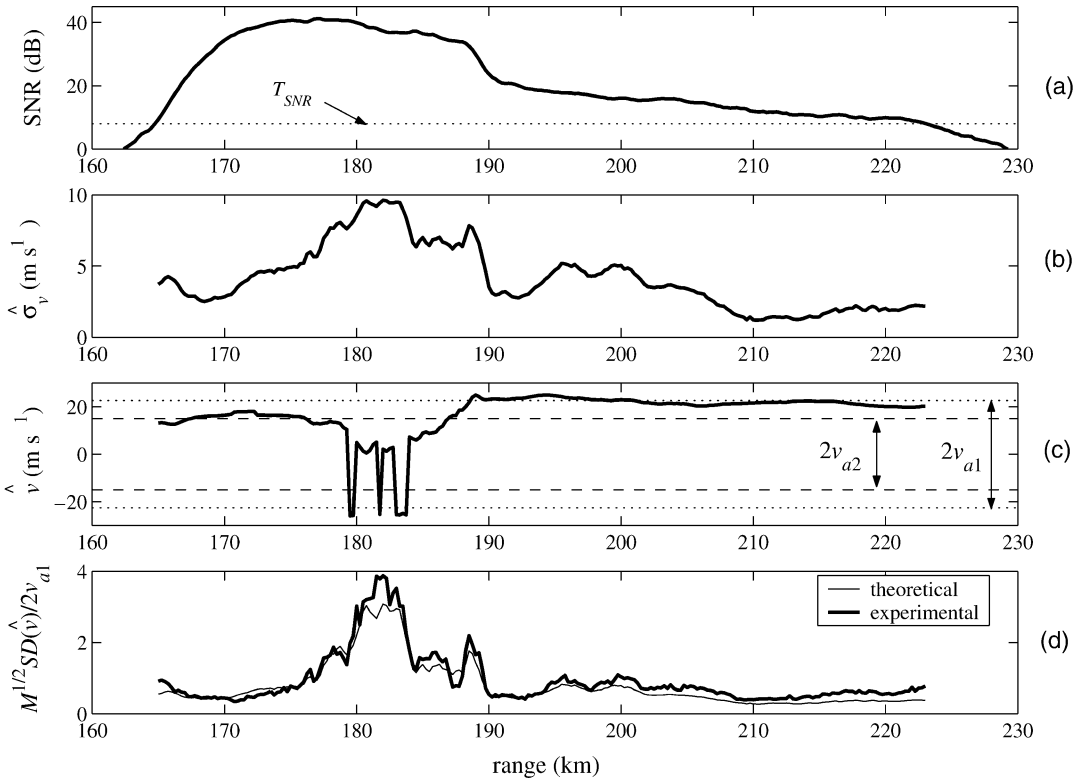

FIG. 5. Statistical performance of the velocity dealiasing algorithm on 200 radials of staggered PRT data collected with a stationary antenna, where $T_1 = 1.6$ ms, $T_2 = 2.4$ ms ($\kappa = 2/3$), $M = 32$, $L' = L = 2$, and $T_{SNR} = 8$ dB. (a) Mean SNR, (b) mean spectrum width, (c) mean Doppler velocity dealiased with the velocity dealiasing algorithm (dotted and dashed lines indicate the Nyquist intervals corresponding to T_1 and T_2, respectively), and (d) experimental and theoretical normalized std devs of velocity estimates.

with NSSL's WSR-88D. The antenna was in a stationary position at an elevation of 1.5°. The staggered PRTs are $T_1 = 1.6$ ms and $T_2 = 2.4$ ms ($\kappa = 2/3$), which lie within the valid region in Fig. 4, and the number of samples is $M = 32$. The number of dealiasing rules was chosen as 5 ($L' = 2$), providing a maximum unambiguous velocity of 45.17 m s^{-1}. Figure 5a shows the mean SNR (over 200 radials) for each range location. Only returns between 160 and 230 km are considered, and just the locations with significant powers are processed; that is, we examine locations where the power is above the SNR threshold T_{SNR} ($T_{SNR} = 8$ dB). Figure 5b shows the mean spectrum width for each range location with significant returns; spectrum widths of up to 10 m s^{-1} can be observed.

The dealiased Doppler velocity is computed for each radial as described in section 2b, and its mean is plotted in Fig. 5c. At some locations, significant differences may be observed among the 200 velocity estimates. This is because all the estimates are not dealiased to the same Nyquist interval (from radial to radial, the estimates of v_1 and v_2 may not be the same due to the time delay between radials and the errors in the autocorrelation estimates, which may lead to catastrophic errors). To avoid unrealistic statistics, the outliers are removed from the data. That is, a histogram of Nyquist interval numbers is computed for the 200 radials, and only the radials in which the dealiased velocity belongs to the predominant Nyquist interval are considered in subsequent analyses. Still, if the determination of the proper Nyquist interval becomes ambiguous because two or more intervals have almost the same propensity of occurrence, a continuity rule is applied, and the predominant Nyquist interval is obtained from the previous range location. Smooth variations in the velocity profile of Fig. 5c confirm that velocity estimates are dealiased to the correct Nyquist interval (after discarding the outliers). Still, a few catastrophic errors occurred between 180 and 185 km, where the spectrum width is in excess of 8 m s^{-1}. Figure 5d depicts the normalized standard deviations of the velocity obtained both from the data and theoretical predictions [cf. (6.21) of Doviak and Zrnić 1993] using the estimated spectrum width (note that unlike the pulse-pair algorithm that uses contiguous pairs, velocity estimates in the staggered PRT technique are obtained with spaced pairs). The plot shows remarkable agreement between the two curves although the theoretical values are slightly smaller within regions of weaker SNRs; this is likely due to excess noise unaccounted for in the calibration. As expected, large errors of ve-

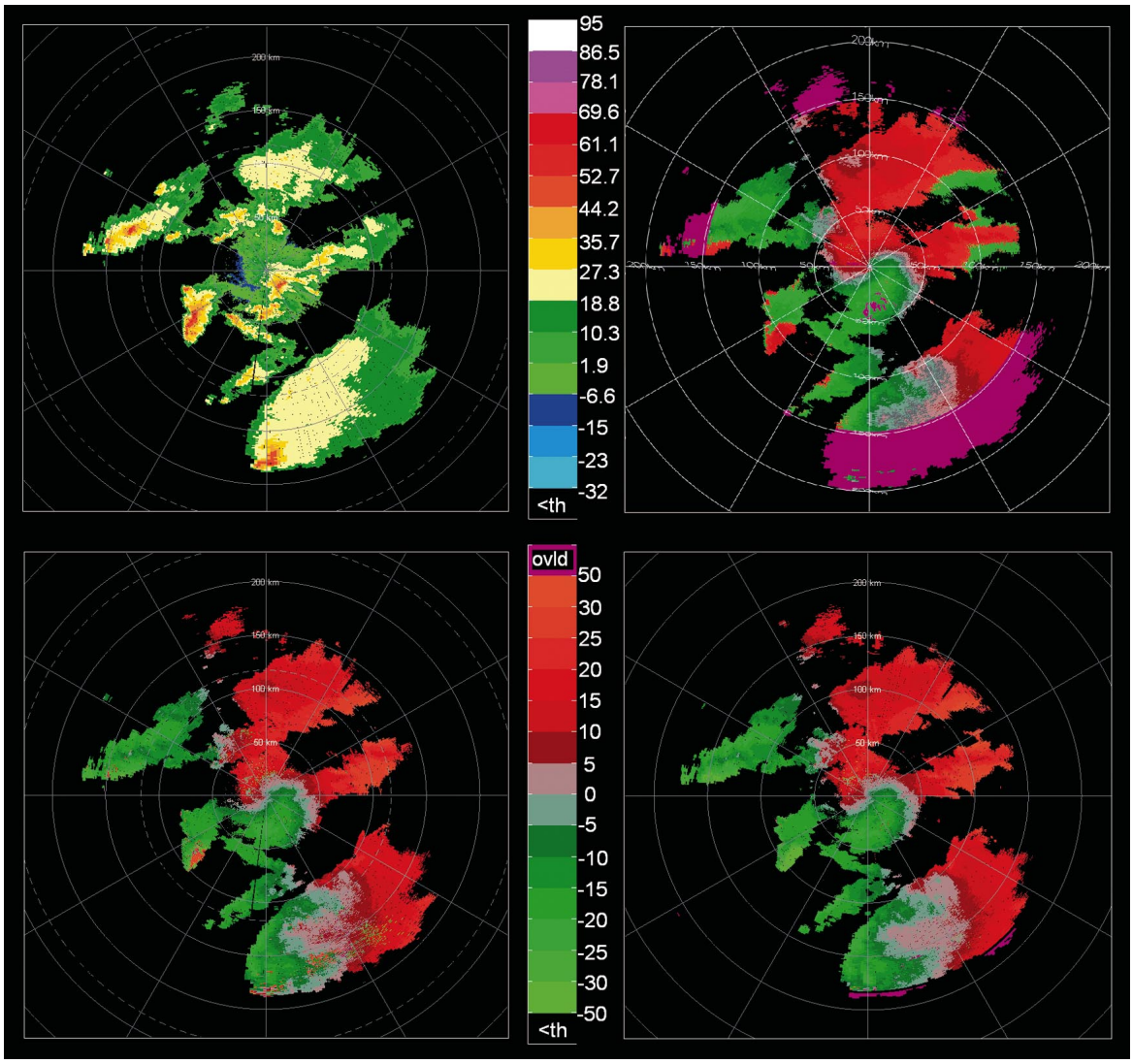

FIG. 6. Displays of severe storms in central Oklahoma obtained at approximately 0445 UTC 6 Apr 2003. (top left) Reflectivity field observed by KOUN with short staggered PRTs (color scale is in dBZ units, black indicates nonsignificant returns). (top right) Doppler velocity field observed by KTLX in the batch mode. (bottom left) Doppler velocity field observed by KOUN with long staggered PRTs. (bottom right) Doppler velocity field observed by KOUN with short staggered PRTs. Velocity color scale is in m s^{-1}, where purple indicates overlaid echoes and black nonsignificant returns. Range rings are 50 km apart.

locity estimates correspond to areas where the spectrum width is large.

c. Results on data

Data collected using the NSSL's KOUN WSR-88D radar in the staggered PRT mode currently consist of nine weather events in central Oklahoma occurring during the fall of 2002 and spring of 2003 (Dubel et al. 2003). These include widespread stratiform precipitation, scattered severe storms, and squall lines. Figure 6 depicts data from approximately 0445 UTC 6 April 2003. On this day, a scattered collection of severe storms developed in Oklahoma, some of which formed distinct clusters. Several cells had reflectivity in excess of 60 dB*Z* and extended to about 350 km from the radar. The radar plan position indicator (PPI) plots displayed in Fig. 6 correspond to an elevation of 2.4° where storms are resolved out to 200 km in range. The top-left panel displays the reflectivity field as observed by the KOUN radar using staggered PRT pulses with $T_1 = 1226.7$ μs and $T_2 = 1840$ μs ($r_{\max}^{(S)} = 276$ km, which is sufficient to observe all echoes with no range ambiguities). The top-right panel shows the Doppler velocity field as observed by the nearby KTLX radar located in Twin Lakes, Oklahoma, about 20 km to the northeast of KOUN. KTLX's Doppler velocities were obtained using the batch mode of the standard precipitation-mode vol-

ume coverage pattern 11 (VCP 11). Due to the presence of strong echoes in the first trip (up to 148 km), most of the second trip is obscured by the purple haze. In addition, some obscuration is observed in the first trip corresponding to stronger second-trip echoes. Because of the limited maximum unambiguous velocity in this mode (v_a = 25.4 m s^{-1}), several areas of velocity aliasing are evident between 100 and 150 km east, northeast, west, and southwest of the radar.

In the bottom panels of Fig. 6 are Doppler velocity fields observed by the KOUN radar using staggered PRTs with a ratio $\kappa = 2/3$. The left panel was obtained with a set of longer PRTs (T_1 = 1600 μs and T_2 = 2400 μs), and the right panel with a set of shorter PRTs (T_1 = 1226.7 μs and T_2 = 1840 μs). Compared with the Doppler velocity field obtained with KTLX (top-right panel of Fig. 6), the staggered PRT scheme results in much cleaner fields with almost no obscuration (depending on the PRTs) given that the maximum unambiguous range for the sets of long and short PRTs is extended to $r_{\max}^{(D)}$ = 184 km and $r_{\max}^{(D)}$ = 240 km, respectively. In addition, the maximum unambiguous velocity obtained with the velocity dealiasing algorithm is v_a = 34.6 m s^{-1} for the set of long PRTs causing few velocity aliases. With the somewhat larger v_a = 41.1 m s^{-1} for the set of short PRTs, there is *no* aliasing. Comparison of the two KOUN Doppler velocity fields also reveals the trade-off between $r_{\max}^{(D)}$ and v_a that is controlled by the PRTs. Whereas longer PRTs (bottom-left panel of Fig. 6) provide more range coverage, they yield a smaller v_a, which results in the occurrence of velocity ambiguities (about 85 km southwest of the radar) and catastrophic errors (about 180 km south and 160 to 170 km southeast of the radar). On the other hand, shorter PRTs (bottom-right panel of Fig. 6) yield a cleaner field (almost no catastrophic errors and no velocity aliasing problems) with limited coverage (purple haze beyond 184 km south and southeast of the radar). A qualitative impression from data in all the events obtained thus far indicates that the longer PRT is quite effective at the elevation of 2.5° and could often be used at the lowest two elevations as well.

5. Conclusions

This paper described the design, real-time implementation, and demonstration of staggered PRT sampling and processing on NSSL's WSR-88D research radar. At the core of the staggered PRT technique is the Doppler velocity dealiasing algorithm, which efficiently uses the fact that Doppler velocities obtained from the short and long PRTs alias in different Nyquist intervals. The design of this algorithm stems from a precise study of the velocity difference transfer function that avoids misconceptions found in previous works. For any staggered PRT ratio of the form $\kappa = m/n$, where m and n are relatively prime integers, the properties of this function lead to a general velocity dealiasing algorithm that extends the maximum unambiguous velocity to its theoretical maximum ($v_a = mv_{a1} = nv_{a2}$). As a result, the maximum unambiguous range and velocity product $r_a v_a$ is m times larger than what is possible with a uniform PRT, improving the ability of weather surveillance radars to observe widespread severe phenomena. However, under practical conditions, it is not always possible to extend v_a to its theoretical maximum due to the unavoidable errors in velocity estimates. The velocity dealiasing algorithm can be modified to operate in a reduced velocity interval to prevent unrealistic dealiasing (catastrophic errors). The larger the errors of velocity estimates, the smaller the effective v_a that can be realized with this technique.

The full algorithm was tailored to allow a seamless insertion into the legacy WSR-88D signal processing pipeline and includes a simple map-based ground clutter filter. Operational tests on the KOUN radar show that the computational complexity of this method is well within the expected capabilities of the next-generation open RDA (ORDA). Although the algorithm is designed to operate with any set of PRTs, factors such as system, range coverage, and echo coherency, limit the choices of PRTs. In general, the best performance is achieved by selecting the set of shortest PRTs satisfying these constraints. These PRTs yield an optimum trade-off between range coverage and maximum unambiguous velocity.

Implementation of the staggered PRT technique on weather radars has been disqualified mainly due to the difficulties in designing efficient ground clutter filters; some new filters have been proposed but are yet to be tested (Sachidananda and Zrnić 2002). Another challenge is spectral processing of nonuniformly sampled time series comprising the staggered PRT sequence. Moreover, because the pulse-pair autocorrelation is obtained from spaced pairs (as opposed to contiguous pairs in the case of uniform PRT), slightly larger standard errors of estimates are expected. Hence, more independent samples may need to be averaged in order to minimize the number of catastrophic errors. This could be accomplished by reducing the antenna rotation rates or with the aid of oversampling and whitening techniques (Torres and Zrnić 2003). Despite these disadvantages, the staggered PRT technique has emerged as a complement to systematic phase coding in the quest to reduce the effects of velocity and range ambiguities on the WSR-88D (Frush et al. 2002).

Preliminary results on weather data demonstrate the performance and prove that the staggered PRT technique is a feasible candidate for mitigating range and velocity ambiguities in future enhancements of the national network of weather surveillance radars. The study of suitable ground clutter filters that achieve the required suppression (Sachidananda and Zrnić 2002) and the evaluation of techniques that extend the range coverage for both reflectivity and Doppler velocity (Sachidananda and Zrnić 2003) are currently under way. Nevertheless,

our current conclusion is that this simple, yet efficient, staggered PRT algorithm is a good replacement of the legacy ''batch mode'' at intermediate elevation angles, where clean separation of overlaid echoes can be easily achieved while extending significantly the unambiguous velocity. This is a definitive advantage at higher elevations where the winds are stronger and hence aliasing is more likely.

Acknowledgments. We would like to thank Chris Curtis for thoroughly reviewing the manuscript and Pengfei Zhang for providing the Doppler velocity PPI from KTLX. Allen Zahrai led the engineering team that performed software and hardware changes to support the real-time implementation of the staggered PRT technique on NSSL's KOUN radar. Igor Ivić completed the synchronizer upgrades, and Chris Curtis was part of the team that developed expanded Volume Coverage Pattern definitions and the tools needed to manipulate the recorded data. The Radar Operations Center of the National Weather Service provided partial support for this work through a Memorandum of Understanding. Funding for this research was provided under NOAA-OU Cooperative Agreement NA17RJ1227.

REFERENCES

Anderson, J. R., 1981: Evaluating ground clutter filters for weather radars. Preprints, *20th Conf. on Radar Meteorology,* Boston, MA, Amer. Meteor. Soc., 314–318.

Chornoboy, E. S., 1993: Clutter filter design for multiple-PRT signals. Preprints, *26th Int. Conf. on Radar Meteorology,* Norman, OK, Amer. Meteor. Soc., 235–237.

Ding, C., D. Pei, and A. Salomaa, 1996: *Chinese Remainder Theorem: Applications in Computing, Coding, Cryptography.* World Scientific Publishing, 213 pp.

Doviak, R. J., and D. S. Zrnić, 1993: *Doppler Radar and Weather Observations.* Academic Press, 562 pp.

——, D. Sirmans, and D. Zrnić, 1976: Resolution of pulse-Doppler radar range and velocity ambiguities in severe storms. Preprints, *17th Conf. on Radar Meteorology,* Seattle, WA, Amer. Meteor. Soc., 15–22.

——, ——, ——, and G. B. Walker, 1978: Considerations for pulse-Doppler radar observations of severe thunderstorms. *J. Appl. Meteor.,* **17,** 189–205.

Dubel, Y. F., S. Torres, and D. Zrnić, cited 2003: Mitigation of range/velocity ambiguities—Staggered PRT algorithm. [Available online at http://cimms.ou.edu/rvamb/Staggered/Stag_Algorithm.htm.]

Frush, C., R. J. Doviak, M. Sachidananda, and D. S. Zrnić, 2002: Application of the SZ phase code to mitigate range–velocity ambiguities in weather radars. *J. Atmos. Oceanic Technol.,* **19,** 413–430.

Gray, G., B. Lewis, J. Vinson, and F. Pratte, 1989: A real-time implementation of staggered PRT velocity unfolding. *J. Atmos. Oceanic Technol.,* **6,** 186–187.

Holleman, I., and H. Beekhuis, 2003: Analysis and correction of dual PRF velocity data. *J. Atmos. Oceanic Technol.,* **20,** 443–453.

Joe, P., and P. T. May, 2003: Correction of dual PRF velocity errors for operational Doppler weather radars. *J. Atmos. Oceanic Technol.,* **20,** 429–442.

——, D. Hudak, J. Scott, R. Passarelli, and A. Siggia, 1997: Operational evaluation of range ambiguity resolution by phase diversity. Preprints, *28th Conf. on Radar Meteorology,* Austin, TX, Amer. Meteor. Soc., 250–251.

Loew, E., and C. A. Walther, 1995: Engineering analysis of dual pulse interval radar data obtained by the ELDORA radar. Preprints, *27th Conf. on Radar Meteorology,* Vail, CO, Amer. Meteor. Soc., 710–712.

Nathanson, F. E., 1969: *Radar Design Principles.* McGraw-Hill, 626 pp.

Papoulis, A., 1984: *Probability, Random Variables, and Stochastic Processes.* 2d ed. McGraw-Hill, 576 pp.

Sachidananda, M., and D. Zrnić, 2000: Clutter filtering and spectral moment estimation for Doppler weather radars using staggered pulse repetition time (PRT). *J. Atmos. Oceanic Technol.,* **17,** 323–331.

——, and ——, 2002: An improved clutter filtering and spectral moment estimation algorithm for staggered PRT sequences. *J. Atmos. Oceanic Technol.,* **19,** 2009–2019.

——, and ——, 2003: Unambiguous range extension by overlay resolution in staggered PRT technique. *J. Atmos. Oceanic Technol.,* **20,** 673–684.

Sirmans, D., D. Zrnić, and B. Bumgarner, 1976: Extension of maximum unambiguous Doppler velocity by use of two sampling rates. Preprints, *17th Conf. on Radar Meteorology,* Seattle, WA, Amer. Meteor. Soc., 23–28.

Torres, S., and A. Zahrai, 2002: Migration of WSR-88D signal processing functionality to open systems. Preprints, *18th Int. Conf. on IIPS,* Orlando, FL, Amer. Meteor. Soc., 5.11.

——, and D. Zrnić, 2003: Whitening in range to improve weather radar spectral moment estimates. Part I: Formulation and simulation. *J. Atmos. Oceanic Technol.,* **20,** 1433–1448.

Zahrai, A., S. Torres, I. Ivic, and C. Curtis, 2002: The open radar data acquisition (ORDA) design for the WSR-88D. Preprints, *18th Int. Conf. on IIPS,* Orlando, FL, Amer. Meteor. Soc., 5.10.

Zrnić, D. S., 1977: Spectral moment estimates from correlated pulse pairs. *IEEE Trans. Aerosp. Electron. Syst.,* **AES-13,** 344–354.

——, and P. Mahapatra, 1985: Two methods of ambiguity resolution in pulse Doppler weather radars. *IEEE Trans. Aerosp. Electron. Syst.,* **21,** 470–483.

——, and R. Cook, 2002: Evaluation of techniques to mitigate range and velocity ambiguities on the WSR-88D. Preprints, *18th Int. Conf. on IIPS,* Orlando, FL, Amer. Meteor. Soc., 5.13.